Multiband Optical Absorption Controlled by Lattice Strain in Thin-Film LaCrO₃

Peter V. Sushko,[1,*] Liang Qiao,[2] Mark Bowden,[2] Tamas Varga,[2] Gregory J. Exarhos,[2] Frank K. Urban III,[3]
David Barton,[3] and Scott A. Chambers[2]

[1]*Department of Physics & Astronomy and the London Centre for Nanotechnology, University College London, Gower Street,
London WC1E 6BT, United Kingdom*
[2]*Pacific Northwest National Laboratory, Richland, Washington 99352, USA*
[3]*Department of Electrical and Computer Engineering, Florida International University, Miami, Florida 33174, USA*
(Received 30 April 2012; published 11 February 2013)

Experimental measurements and *ab initio* modeling of the optical transitions in strained *G*-type antiferromagnetic LaCrO₃ resolve two decades of debate regarding the magnitude of the band gap and the character of the optical absorption spectrum in the visible-to-ultraviolet (up to ∼5 eV) range in this material. Using time-dependent density functional theory and accounting for thermal disorder effects, we demonstrate that the four most prominent low-energy absorption features are due to intra-Cr t_{2g}-e_g (2.7, 3.6 eV), inter-Cr t_{2g}-t_{2g} (4.4 eV), and interion O $2p$-Cr $3d$ (from ∼5 eV) transitions and show that the excitation energies of the latter type can be strongly affected by the lattice strain.

Complex oxide heterostructures may exhibit properties not observed in the bulk phases of the individual constituents. Accordingly, it is of interest to engineer structures with novel optical properties by combining materials with specific electronic structure features and utilizing their response to lattice strain. However, it is essential to first understand the detailed nature of the optical absorption (OA) bands and effect of strain on these individual complex oxides.

This Letter reports a joint experimental and theoretical study of the OA in *G*-type antiferromagnetic perovskite LaCrO₃ (LCO) and reveals the effect of strain on the OA in this and related materials.

Optical reflectivity measurements [1] put the onset of the optical gap in LCO at ∼3.4 eV and concluded that the band at ∼4 eV was sufficiently intense to characterize it as the O $2p$-Cr $3d$ charge transfer band, while the Cr d-d transitions were found to be indiscernible. According to the ultraviolet photoemission and Bremsstrahlung isochromat spectroscopic measurements [2], the value of the intrinsic band gap is 2.8 eV, which was concluded to be within the experimental error of the 3.4 eV value from Ref. [1]. On the modeling side, recent calculations, based on density functional theory (DFT), reported Cr t_{2g}-e_g transitions at 1.40 and 2.15 eV, a reflectivity peak at 2.38 eV, and the onset of the O $2p$-Cr $3d$ transitions at 3.4 eV, of which only the latter absorption feature has been observed experimentally [3]. Other calculations yield band gap values between 0.6 and 4.5 eV depending on the computational method used (see Ref. [3] for details). Such lack of consistency between the experimental and theoretical results is a major roadblock to the rational design and fabrication of oxide heterostructures and exploitation of their properties.

In contrast to earlier studies, we use compositionally and structurally well-defined LCO films and—for *ab initio*

simulations—an embedded cluster method [4], together with a hybrid density functional, which provides a reliable description of band gaps. The main conclusions of our study are (i) the LCO OA spectrum contains distinct contributions associated with intra-Cr $t_{2g} \rightarrow e_g$, inter-Cr $t_{2g} \rightarrow t_{2g}$, and O $2p \rightarrow$ Cr $3d$ transitions, (ii) the onset of the O $2p$-Cr $3d$ charge transfer gap is between 4.6 and 5.0 eV, and (iii) the magnitude of the charge-transfer gap depends on the lattice strain, while the energies of the Cr d-d transitions are strain insensitive. In addition, we demonstrate that qualitative behavior of the OA bands can be predicted from the structural parameters of the strained LCO alone. These results present LCO in a very different light than has been done previously. Importantly, this approach can be generalized to other multiband materials exhibiting complex OA spectra.

A description of the film samples used in the experimental part of this investigation can be found elsewhere [5–7]. Optical excitation energies were calculated using an embedded cluster method in which a finite cluster is treated quantum mechanically and embedded into the electrostatic potential produced by the lattice [4,8]. Clusters containing one, two (linear), four (planar), and eight (cubic) Cr atoms have been considered. These are denoted as Cr × 1, Cr × 2, Cr × 4, and Cr × 8, respectively. The excitation energies (ϵ) and the corresponding oscillator strengths (f) were calculated using the time-dependent DFT method and a density functional by Tao *et al.* [9] implemented in the GAUSSIAN 09 code [10]. The OA spectra were simulated as a convolution of functions $f_n \exp[(\epsilon - \epsilon_n)^2/a^2]$ ($n =$ 1–30) for the lowest-energy transitions of each type. The constant a is selected so that the full width at half of the maximum is 0.2 eV for each function. To model thermal disorder effects, we performed a constant energy molecular dynamics (MD) simulation of bulk LCO at ∼200 K. The

OA spectra were calculated for ten MD configurations, separated by 0.5 ps, and convoluted to obtain an averaged spectrum. See Ref. [6] for details.

The lowest-energy electronic configuration of LCO corresponds to the G-type magnetic ordering in all our calculations. Each Cr^{3+} ion has three occupied t_{2g} states in high-spin configuration and hybridized with $2p$ states of neighboring oxygen atoms, while the three other t_{2g} states and all e_g states are vacant. This splits the Cr sites into two equivalent sublattices $Cr\uparrow$ and $Cr\downarrow$, shown in Figs. 1(a) and 1(b), in which the t_{2g} electrons are in spin-up and spin-down states, respectively. Figure 1(c) shows the total density of states (DOS) and the DOS projected on the t_{2g} and e_g states calculated using the periodic model, a Gaussian-type basis set and the B3LYP density functional, as implemented in the CRYSTAL09 package [11]. For the spin-up electrons [top panel of Fig. 1(c)], occupied $Cr\uparrow t_{2g}$ states form the lowest energy Cr $3d$ subband. It is followed, in order of increasing energy, by the vacant $Cr\uparrow e_g$ (with a minor contribution of $Cr\downarrow e_g$), $Cr\downarrow t_{2g}$, and, finally, $Cr\downarrow e_g$ (with a minor contribution of $Cr\uparrow e_g$) states. Thus, the Cr $3d$ states split into four subbands [Fig. 1(d)], which we will denote as $t_{2g}(o)$ and $t_{2g}(v)$ for *occupied* and *virtual* and $e_g(l)$ and $e_g(h)$ for *low* and *high*. All other unoccupied states are assigned to the conduction band (CB). This electronic structure gives rise to eight types of spin-allowed optical excitations shown in Fig. 1(d).

The absorption coefficient, including a contribution due to the index mismatch at the air-film and film-substrate interfaces, obtained experimentally for the LCO on a-SiO$_2$ is shown in Fig. 2(a). Its structure is indicative of a superposition of several absorption bands, as discussed above. Characteristic features of this spectrum include weak peaks at 2.7(1) and 3.6(1) eV, a steep rise at $\sim$4 eV, an even steeper rise at $\sim$5 eV, and clearly visible knee-like features at $\sim$5.2, $\sim$5.5, and $\sim$6.5 eV and a broad feature at $\sim$2 eV. To isolate the index mismatch contribution, we turn to spectroscopic ellipsometry (SE), which allows the index of refraction and extinction coefficient to be independently determined for the bare substrate and the substrate-plus-film system. Figure 2(b) shows the extinction coefficient for 50 nm of epitaxial LCO on SrTiO$_3$(001) after a linear background subtraction based on a linear least-squares fit of the data from 1.3 to 2.0 eV. The data were collected to the highest photon energy available with the SE system. The spectrum is well-fitted to Gaussians centered at 2.7(1) and 3.8(1) eV. These energies are within experimental error of those determined by fitting the weak features over the same energy range in the LCO/a-SiO$_2$ (2.7(1) and 3.6(1) eV), which indicates that these bands are independent of the strain state. The SE spectrum shows no statistically significant signal below 2.2 eV, which suggests that the broad feature near 2 eV in Fig. 2(a) originates not from absorption, but from the index mismatches at the various interfaces [6].

The overall fit of the absorption coefficient [Fig. 2(a)] to this family of Gaussians is excellent. However, the fit alone does not reveal the origin of the transitions involved and may present an incorrect physical picture. To make a preliminary assignment of these bands, we calculated the excitation energies for each of the eight types of the transitions shown in Fig. 1(d) using the ideal cubic LCO lattice structure and Cr $\times$ 2 cluster. Three of these types

FIG. 1 (color online).   Geometrical structure of bulk LaCrO$_3$ and spin densities for sublattices of the spin-up $Cr\uparrow$ (a) and spin-down $Cr\downarrow$ (b) sites. (c) Total density of states and its projection on the d states of $Cr\uparrow$ (light color, yellow) and $Cr\downarrow$ (dark color, blue) sublattices. (d) Schematics of the Cr $3d$ bands and spin-allowed optical transitions—four from the occupied t_{2g} states (open red arrows) and four from the O $2p$ band (blue shaded arrows).

FIG. 2 (color online).   (a) Experimental OA spectrum measured for LCO on a-SiO$_2$ and fitted to seven Gaussians. The shaded Gaussians represent intra- and inter-Cr d-d transitions, as assigned on the basis of *ab initio* simulations. (b) Spectroscopic ellipsometry measurement of the extinction coefficient for LCO/SrTiO$_3$(001) after background subtraction. Positions of all Gaussians in (a), except for the index mismatch contribution at 2.0 eV, are shown with arrows.

are due to Cr d-d transitions: intra-Cr $t_{2g}(o) \to e_g(l)$ and inter-Cr $t_{2g}(o) \to t_{2g}(v)$ and $t_{2g}(o) \to e_g(h)$. The $t_{2g}(o) \to e_g(l)$ transitions split into two groups. The lower-energy group (2.8 eV) is due to d_{xy}-$d_{x^2-y^2}$, d_{xz}-d_{z^2}, and d_{yz}-d_{z^2} transitions, in which the spatial separation between the excited electron and the corresponding hole is smaller and, therefore, the electrostatic interaction between them is stronger. The higher-energy group (3.4 eV) is due to the transitions for which such interaction is weaker: d_{xy}-d_{z^2}, d_{xz}-$d_{x^2-y^2}$, d_{yz}-$d_{x^2-y^2}$. The calculated inter-Cr $t_{2g}(o) \to t_{2g}(v)$ and $t_{2g}(o) \to e_g(h)$ transitions are at $\sim$4.6 and 5.9 eV, respectively. Importantly, there is good agreement between the calculated excitation energies for the d-d transitions and the bands at 2.7(1), 3.6(1), and 4.40(1) eV in Fig. 2(a) and those at 2.7(1) and 3.8(1) eV in Fig. 2(b), which makes a case for the assignment of these bands. We note that the 2.7 eV absorption band is consistent with the green color of LCO samples, as observed elsewhere [12]. Although the calculated excitation energy of the inter-Cr $t_{2g}(o) \to e_g(h)$ transitions matches well the Gaussian centered at 5.54(3) eV, a definite assignment of this band is impossible due to the overlap with other transitions in the same energy range.

The remaining five types of the optical transitions involve delocalized states of the O $2p$ and conduction bands. We calculate 30 excited states of each type, which is sufficient to determine the onsets of the excitation energies and relative intensities of the corresponding absorption bands. According to these calculations, O $2p \to e_g(l)$ transitions provide the dominant contribution among the five types and their onset energy is at $\sim$5 eV, which is consistent with the steep rise near 5 eV in the experimental spectrum [Fig. 2(a)].

The results obtained using the ideal LCO lattice and Cr $\times$ 2 cluster are incomplete in two senses. First, these results do not account for thermal fluctuations, which affect relative intensities of the OA bands. For example, the intensity of $t_{2g}(o) \to e_g(l)$ peaks has to be scaled by a factor of 200 to make the ratio of intensities $I_{t_{2g}\text{-}t_{2g}}/I_{t_{2g}\text{-}e_g}$ comparable to measured ratios $I_{4.40}/I_{3.6}$ and $I_{4.40}/I_{2.7}$. Second, the energies of transitions involving delocalized states depend on the cluster size [13,14]; i.e., the values obtained using the Cr $\times$ 2 cluster alone are not reliable. Both of these issues need to be addressed in order to reach quantitative agreement between theory and experiment.

To account for finite temperatures, we have calculated the OA spectra for the orthorhombic and pseudocubic LCO ($a = 3.8840$ Å) [6] using Cr $\times$ 4 clusters and averaged these spectra over 10 thermally disordered LCO configurations. To improve statistical averaging, each spectrum was additionally averaged over the cluster orientations in a-b, b-c, and c-a lattice planes. Here, we focussed on the most prominent absorption features: the intra-Cr $t_{2g}(o) \to e_g(l)$, inter-Cr $t_{2g}(o) \to t_{2g}(v)$, and O $2p \to e_g(l)$ transitions.
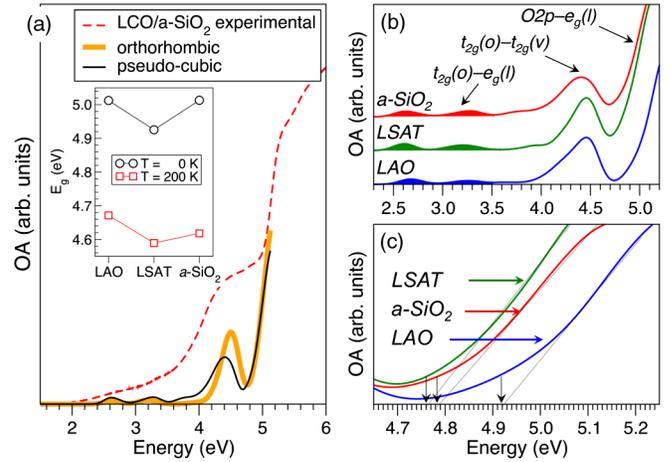
FIG. 3 (color online).   (a) Observed and calculated OA spectra for unstrained LCO. (b) Calculated OA spectra for pseudocubic unstrained (a-SiO$_2$) and strained (LSAT, LAO) LCO. (c) Onset of the O $2p \to e_g(l)$ transitions. Vertical arrows indicate E_g values. Experimental lattice cell parameters and Cr $\times$ 4 clusters were used in all cases. Inset in (a) shows the values of E_g extrapolated to infinite cluster size.

The calculated absorption spectra are compared to the experimental OA spectrum for LCO/a-SiO$_2$ in Fig. 3(a). The broad index-mismatch feature at $\sim$2 eV has been removed for this comparison. The positions and relative intensities of the $t_{2g}(o) \to e_g(l)$ and $t_{2g}(o) \to t_{2g}(v)$ bands are in reasonable agreement with experiment. We note that the spectra calculated for the orthorhombic and pseudocubic LCO are nearly identical except in the 3.6–4.7 eV range, which corresponds to the inter-Cr $t_{2g}(o) \to t_{2g}(v)$ transitions. This indicates that the amplitude of thermal fluctuations, such as those associated with rotation of the lattice octahedra, is larger in pseudocubic than in orthorhombic LCO, as expected. In order to make consistent comparison across the series of strained supported LCO films, we will take the pseudocubic structure as a reference for unstrained LCO.

Figure 3(b) compares the OA spectrum found for pseudocubic unstrained LCO (a-SiO$_2$) and those for the LCO under 0.4 and 1.2% residual compressive strain, as in LCO/LSAT (001) and LCO/LAO(001), respectively. All spectra have been calculated following the same procedure. One can see that the positions, widths, and relative intensities of the Cr d-d absorption bands are in good agreement with those for $\sim$2.7, $\sim$3.6, and $\sim$4.4 eV bands observed experimentally in LCO/a-SiO$_2$ (Fig. 2). We emphasize that thermal fluctuations break the symmetry of Cr $3d$ states and make $t_{2g}(o) \to e_g(l)$ transitions weakly allowed. The shape of the $t_{2g}(o) \to t_{2g}(v)$ band changes as the magnitude of the compressive strain increases: the peak shifts slightly to the higher energy, as in orthorhombic LCO, and the low-energy tail becomes longer. This is consistent with the expected smaller magnitude of the thermal fluctuations in the a-b plane and larger magnitude of these fluctuations along the c axis.

To investigate the cluster size effect on the onset of the O $2p \rightarrow e_g(l)$ transitions, we define the charge transfer optical band gap (E_g) by extrapolating the low-energy tail of this band to the abscissa axis [Fig. 3(c)]. The values of $E_g(N)$ were calculated using $Cr \times N$ ($N = 1, 2, 4, 8$) clusters at zero temperature (see Ref. [6] for details) and extrapolated to $N = \infty$ using $E_g(N) = E_g + A \exp(-BN)$, where E_g, A, and B are fitting parameters. Then, a shift of the magnitude $\Delta E = E_g - E_g(4)$ was applied to correct the O $2p \rightarrow e_g(l)$ part of the finite-temperature OA spectra shown in Fig. 3(b). The values of E_g at $T = 0$ K and $T = 200$ K for all three strain states are shown in the inset in Fig. 3(a). These data suggest that E_g calculated using $Cr \times 4$ clusters are overestimated by ~0.2 eV. On the contrary, dependence of the Cr d-d transition energies on the cluster size is negligible [6].

To reconcile a relatively strong effect of the substrate on E_g and a lack of this effect on the $t_{2g}(o) \rightarrow e_g(l)$ and $t_{2g}(o) \rightarrow t_{2g}(v)$ transitions, we note that the positions of the Cr $3d$ states with respect to the O $2p$ band are influenced by two structural parameters: the cell volume (V) and the tetragonality ratio ($t = c/a$). Indeed, the larger the V, the larger the interatomic distances and, therefore, the smaller the repulsion between the Cr $3d$ and O $2p$ electrons. Thus, as V increases, the Cr $3d$ states shift closer to the top of the O $2p$ band. On the other hand, as the value of t increases, the t_{2g} and the e_g bands become wider and the gap between them—smaller.

These effects are illustrated in Fig. 4 for the one-electron energy differences calculated using the same method as the data in Fig. 1(c). For a given t, the gap between O $2p$ and $e_g(l)$ decreases sharply as V increases, while the gap between $t_{2g}(o)$ and $e_g(l)$ is hardly affected [Fig. 4(a)].
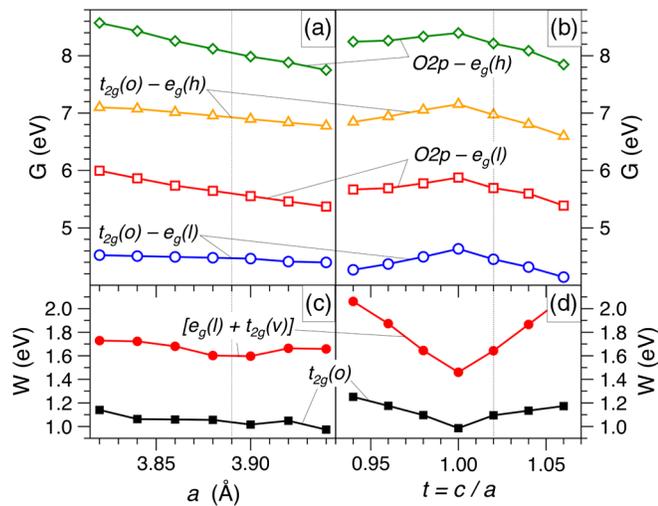
FIG. 4 (color online). Effect of lattice strain on the one-electron band gaps G (a),(b) and the width of the bands W (c), (d). Vertical lines show the a lattice parameter (a),(c) and the tetragonality ratio (b),(d) in LaCrO$_3$ supported on LaAlO$_3$ (001).

In addition, the width of the $t_{2g}(o)$ subband and the combined width of the $e_g(l)$ and $t_{2g}(v)$ subbands show little dependence on the value of V [Fig. 4(c)]. In contrast, when the V is fixed and the t is changed [Figs. 4(b) and 4(d)], the gaps and the widths of the Cr $3d$ subbands show a characteristic dependence, such that the maximum of the gaps and the minimum of the band widths are found for $t = 1$.

To apply these considerations, we notice that the cell volumes of LCO on LAO and LSAT are $V_{LAO} = 57.64$ Å^3 and $V_{LSAT} = 58.89$ Å^3; i.e., they differ by over 2.1%. At the same time, their tetragonality ratios are nearly the same: $t_{LAO} = 1.019$ and $t_{LSAT} = 1.016$. Thus, according to Fig. 4(a), the O $2p$-$e_g(l)$ gap in LCO/LSAT should be lower than that in LCO/LAO. This is, indeed, what we find from the calculations of the excited states. On the other hand, since $t_{SiO_2} = 1$ and $t_{LSAT} > 1$, the O $2p$-$e_g(l)$ gap in LCO/a-SiO$_2$ should be larger than that in LCO/LSAT [Fig. 4(c)] even though the V_{SiO_2} (58.59 Å^3) is close to V_{LSAT}. This is apparent in our calculations at $T = 0$ K [see inset in Fig. 3(c)] but the effect of tetragonality seems to become less pronounced at finite T. One can expect that these trends apply to all isostructural materials, thus making it possible to predict modifications of the OA spectra in strained perovskites by screening their ground state electronic structure and elastic properties.

To summarize, we investigated OA in G-type antiferromagnetic LCO and assigned the four most prominent low-energy absorption features. In particular, our results reveal that the feature at ~4 eV, mistakenly taken as the O $2p$-Cr $3d$ charge transfer gap in the earlier studies, is a prominent inter-Cr t_{2g}-t_{2g} transition, which can be considered as a Mott-type transition. Instead, the O $2p$-Cr $3d$ gap in this material is between 4.6 and 5 eV, i.e., about 1 eV higher than previously thought. Our results for strained LCO lead us to conclude that the positions of some of the bands can be affected selectively and that band gap changes of ~0.2 eV can be achieved by judiciously choosing the strain conditions. The strain-induced modifications can be described using two structural parameters—the cell volume and tetragonality ratio, which suggests that the Poisson's ratio of a material determines its band gap sensitivity to the lattice strain. It follows from these calculations that interfaces of two G-type antiferromagnets containing transition metals will give rise to more complex d-type subbands, resulting in more complex OA spectra. We propose that low-energy optical transitions leading to conductivity under infrared irradiation can be realized in such interfaces.

*Corresponding author.
p.sushko@ucl.ac.uk

[1] T. Arima, Y. Tokura, and J. B. Torrance, Phys. Rev. B **48**, 17 006 (1993).

[2] K. Maiti and D. D. Sarma, Phys. Rev. B **54**, 7816 (1996).

[3] K. P. Ong, P. Blaha, and P. Wu, Phys. Rev. B **77**, 073102 (2008).

[4] D. Muñoz Ramo, P. V. Sushko, J. L. Gavartin, and A. L. Shluger, Phys. Rev. B **78**, 235432 (2008).

[5] L. Qiao, T. C. Droubay, M. E. Bowden, V. Shutthanandan, T. C. Kaspar, and S. A. Chambers, Appl. Phys. Lett. **99**, 061904 (2011).

[6] See Supplemental Material at http://link.aps.org/supplemental/10.1103/PhysRevLett.110.077401 for descriptions of the samples, experimental procedures, and details of the calculations.

[7] S. A. Chambers, L. Qiao, T. C. Droubay, T. C. Kaspar, B. W. Arey, and P. V. Sushko, Phys. Rev. Lett. **107**, 206802 (2011).

[8] P. V. Sushko and I. V. Abarenkov, J. Chem. Theory Comput. **6**, 1323 (2010).

[9] J. Tao, J. P. Perdew, V. N. Staroverov, and G. E. Scuseria, Phys. Rev. Lett. **91**, 146401 (2003).

[10] M. J. Frisch, G. W. Trucks, H. B. Schlegel, G. E. Scuseria, M. A. Robb, J. R. Cheeseman, G. Scalmani, V. Barone, B. Mennucci, G. A. Petersson *et al.*, GAUSSIAN 09 Revision A.2 (Gaussian Inc., Wallingford, CT, 2009).

[11] R. Dovesi, V. R. Saunders, C. Roetti, R. Orlando, C. M. Zicovich-Wilson, F. Pascale, B. Civalleri, K. Doll, N. M. Harrison, I. J. Bush *et al.*, CRYSTAL09 User's Manual (University of Torino, Torino, 2009).

[12] K. Hayashi, S. Matsuishi, T. Kamiya, M. Hirano, and H. Hosono, Nature (London) **419**, 462 (2002).

[13] P. V. Sushko, A. L. Shluger, and C. R. A. Catlow, Surf. Sci. **450**, 153 (2000).

[14] N. Govind, P. V. Sushko, W. P. Hess, M. Valiev, and K. Kowalski, Chem. Phys. Lett. **470**, 353 (2009).